AGU PUBLICATIONS

JGR

Journal of Geophysical Research: Solid Earth

RESEARCH ARTICLE
10.1002/2014JB011580

Key Points:
- Low velocities beneath the volcanic line from the base of the crust to 200 km
- Vertical boundary between velocities beneath the volcanic line and the craton
- Low velocities shallow as the Moho, showing alteration of lithospheric mantle

Supporting Information:
- Figures S1 and S2

Correspondence to:
A. N. Adams,
aadams@seismo.wustl.edu

Citation:
Adams, A. N., D. A. Wiens, A. A. Nyblade, G. G. Euler, P. J. Shore, and R. Tibi (2015), Lithospheric instability and the source of the Cameroon Volcanic Line: Evidence from Rayleigh wave phase velocity tomography, *J. Geophys. Res. Solid Earth*, *120*, doi:10.1002/2014JB011580.

Received 29 AUG 2014
Accepted 11 FEB 2015
Accepted article online 16 FEB 2015

Lithospheric instability and the source of the Cameroon Volcanic Line: Evidence from Rayleigh wave phase velocity tomography

Aubreya N. Adams[1], Douglas A. Wiens[1], Andrew A. Nyblade[2], Garrett G. Euler[3], Patrick J. Shore[1], and Rigobert Tibi[4]

[1]Department of Earth and Planetary Sciences, Washington University in St. Louis, Saint Louis, Missouri, USA, [2]Department of Geosciences, Penn State University, University Park, Pennsylvania, USA, [3]Los Alamos National Laboratory, New Mexico, USA, [4]Global Geophysical Services, Inc., Denver, Colorado, USA

Abstract The Cameroon Volcanic Line (CVL) is a 1800 km long volcanic chain, extending SW-NE from the Gulf of Guinea into Central Africa, that lacks the typical age progression exhibited by hot spot-related volcanic tracks. This study investigates the upper mantle seismic structure beneath the CVL and surrounding regions to constrain the origin of volcanic lines that are poorly described by the classic plume model. Rayleigh wave phase velocities are measured at periods from 20 to 182 s following the two-plane wave methodology, using data from the Cameroon Seismic Experiment, which consists of 32 broadband stations deployed between 2005 and 2007. These phase velocities are then inverted to build a model of shear wave velocity structure in the upper mantle beneath the CVL. Results show that phase velocities beneath the CVL are reduced at all periods, with average velocities beneath the CVL deviating more than −2% from the regional average and +4% beneath the Congo Craton. This distinction is observed for all periods but is less pronounced for the longest periods measured. Inversion for shear wave velocity structure indicates a tabular low velocity anomaly directly beneath the CVL at depths of 50 to at least 200 km and a sharp vertical boundary with faster velocities beneath the Congo Craton. These observations demonstrate widespread infiltration or erosion of the continental lithosphere beneath the CVL, most likely caused by mantle upwelling associated with edge-flow convection driven by the Congo Craton or by lithospheric instabilities that develop due to the nearby edge of the African continent.

1. Introduction

The Cameroon Volcanic Line (CVL) is a 1800 km long SW-NE trending linear chain of volcanic centers that extends from the Gulf of Guinea to onshore central Cameroon (Figure 1). Numerous studies have noted that the CVL does not display a clear age progression along the line as is exhibited by "typical" hot spot chains [e.g., *Hedberg*, 1969; *Grant et al*., 1972; *Grunau et al*., 1975; *Dunlop and Fitton*, 1979; *Cornen and Maury*, 1980; *Dunlop*, 1983; *Fitton and Dunlop*, 1985; *Lee et al*., 1994; *Ngounouno et al*., 1997; *Marzoli et al*., 1999, 2000; *Ngounouno et al*., 2001, 2003; *Njilah et al*., 2004; *Ngounouno et al*., 2005, 2006; *Aka et al*., 2009; *Dongmo et al*., 2010; *Kamgang et al*., 2010; see *Njome and de Wit*, 2014, Figure 2]. The absence of age progression along the line has led to much debate over the geodynamic origin of this feature, with suggested formation mechanisms ranging from multiple mantle plumes [*Ngako et al*., 2006], to reactivation of previously existing shear zones [*Ebinger and Sleep*, 1998], to mantle upwellings driven by convection currents of various sources [*King and Anderson*, 1995, 1998; *Meyers et al*., 1998; *King and Ritsema*, 2000].

In this study, we present images of upper mantle structure beneath Cameroon and the surrounding regions to evaluate the proposed candidate models for the origin of the CVL. We measure phase velocities from 32 broadband stations deployed during 2005–2007 at a range of periods sensitive to upper mantle depths. These phase velocities are then inverted for three-dimensional upper mantle shear wave velocity structure. This methodology provides better depth resolution and imaging of the shallow upper mantle than was possible for earlier body wave tomography studies (see section 2.3) and provides strong constraints on the shape, orientation, and depth extent of the low velocity anomaly (LVA) beneath the CVL. We suggest that this low velocity anomaly is associated with the magma source regions for the CVL and use these observations to evaluate the viability of previously proposed models. Finally, we discuss the implications of the new results for the dynamics of the CVL.

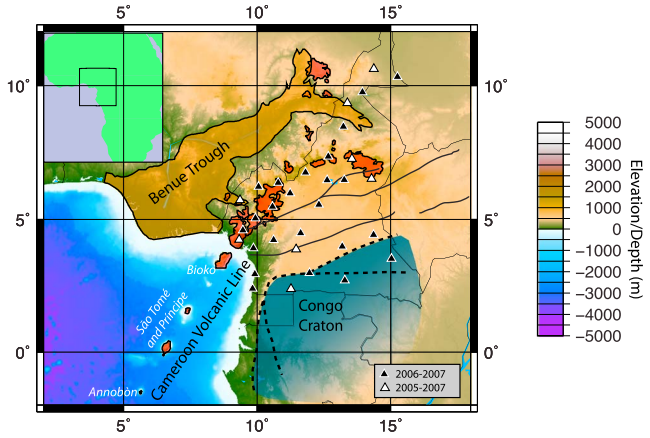

Figure 1. Map showing major geologic features and the locations of seismic stations used in this study. Surficial exposures of volcanic materials associated with the CVL are shown in red, while the Benue Trough is shown in orange, and the Congo Craton is shown in blue. Dashed lines along the northern and western boundaries of the Congo Craton indicate areas where the boundary is not well defined. Bold black lines between the CVL and the Congo Craton indicate major shear zones associated with the CASZ. Pale gray lines throughout the figure show country borders. Locations of seismic stations used in this study are shown by colored triangles. White triangles indicate stations that were installed in 2005, while black triangles show stations that were installed in 2006. Latitude and longitudes for all stations are given in *Koch et al.* [2012].

2. Geologic Setting and Previous Work

2.1. The Cameroon Volcanic Line

The CVL trends N30°E and includes multiple volcanic and plutonic centers and associated zones of uplift, which are split into an oceanic and a continental sector of roughly equal lengths (Figure 1). The oceanic sector of the CVL extends from Annobòn (Pagalú) in the southwest to Bioko in the northeast, encompassing the island nation of São Tomé and Principe. The onshore sector of the CVL consists of seven primary volcanoes including Mt. Cameroon near the coast and extending farther to the east within central Cameroon [*Déruelle et al*., 2007]. Further to the northeast, the CVL bifurcates, with one branch extending approximately 300 km north to the Biu Plateau in northeastern Nigeria. The second branch extends 200 km east through the Adamawa Plateau. Volcanic islands and seamounts are superimposed on a 200 km wide, 3 km high asymmetric crustal arch parallel to the trend of the CVL [*Meyers et al*., 1998]. A similar uplift of 1 km, the Adamawa Uplift, is also observed beneath the continental portion of the CVL [*Meyers et al*., 1998].

The earliest igneous activity associated with the CVL consisted of the intrusion of more than 60 alkaline plutonic ring complexes 66–30 Ma [*Déruelle et al*., 1991, 2007]. Volcanism in the continental CVL began 42 Ma, while offshore volcanic activity initiated 30 Ma and is interpreted to be synchronous with the uplift of the crustal arch [*Grunau et al*., 1975; *Meyers and Rosendahl*, 1991; *Meyers et al*., 1998]. Volcanism continues to the present at both onshore and offshore volcanic centers. Although there is no evidence for age progression of volcanics along the onshore portion of the CVL [e.g., *Hedberg*, 1969; *Grant et al*., 1972; *Grunau et al*., 1975; *Dunlop and Fitton*, 1979; *Cornen and Maury*, 1980; *Dunlop*, 1983; *Fitton and Dunlop*, 1985; *Lee et al*., 1994; *Ngounouno et al*., 1997; *Marzoli et al*., 1999, 2000; *Ngounouno et al*., 2001, 2003; *Njilah et al*., 2004; *Ngounouno et al*., 2005, 2006; *Aka et al*., 2009; *Dongmo et al*., 2010; *Kamgang et al*., 2010], some studies have suggested a possible seaward progression for the oceanic sector; however, this possibility remains unclear due to small numbers of samples [*Grunau et al*., 1975; *Meyers and Rosendahl*, 1991; *Meyers et al*., 1998]. Figure 2 in *Njome and de Wit* [2014] offers a detailed summary of volcanic ages and compositions across the CVL.

Volcanics throughout the CVL consist primarily of alkaline basalts [*Hedberg*, 1969]. Sr and Nd isotopic studies yield similar results for both the continental and oceanic volcanic centers, suggesting that volcanics in both sectors came from the same sublithospheric source [*Déruelle et al*. 2007]. Ultramafic xenoliths are found in multiple locations in the CVL, further strengthening the case for a mantle source of the CVL volcanics [e.g., *Déruelle et al*., 1991; *Princivalle et al*., 2000; *Déruelle et al*., 2007].

2.2. The Regional Geologic Setting

The basement of the CVL and most of northern Cameroon is the Oubanguides Belt, part of the Pan-African belt formed by the collision of the São Francisco, Congo, and West African Cratons during the Neoproterozoic formation of Gondwana. Several shear zones exist within the Oubanguides Belt, most notably the Central African Shear Zone (CASZ), which extends eastward to the Darfur region in Sudan and is associated with the

Pernambuco lineament in Brazil [e.g., *Burke et al*., 1971; *Browne and Fairhead*, 1983; *Dorbath et al*., 1986; *Fairhead and Okereke*, 1987; *Fairhead and Binks*, 1991].

The CVL is bordered to the north by the Benue Trough, a Cretaceous rift, whose shape and orientation parallel that of the CVL. The formation of the Benue Trough was temporally associated with the opening of the Atlantic Ocean, beginning 140 Ma and continuing until 84 Ma, followed by a period of compression. Magmatic activity was present 147–106 Ma in the northern Benue Trough and 97–9 Ma in the southern Benue Trough [*Maluski et al*., 1995]. Volcanics throughout the Benue Trough are primarily alkaline and tholeiitic basalts [*Coulon et al*., 1996, and references therein]. The similarities in shape, orientation, and volcanic composition between the Benue Trough and the CVL have led many researchers to suggest a related origin for both features [e.g., *Fitton*, 1980, 1987], but a plausible common mechanism has yet to be proposed.

To the south, the CASZ within the Oubanguides Belt separates the CVL from the Congo Craton. The Archean to Paleoproterozoic Congo Craton constitutes a large portion of central and southern Africa, and is one of several large pre-Cambrian cratons that make up the African continent. The northwestern portion of the Congo Craton, the Ntem Complex, is exposed in southern Cameroon [*Vicat et al*., 1996]. At the northern boundary of the Congo Craton, Pan-African rocks from the Oubanguides Belt have overthrust the Ntem Complex, creating difficulty in defining the northern boundary of the Congo Craton based solely upon surficial geology [*Boukeke*, 1994]. One recent study of crustal structure, however, found evidence of a crustal suture, which may indicate the boundary of this terrain [*Tokam et al*., 2010].

2.3. Previous Geophysical Studies

A 5-month study by the University of Leeds and ORSTOM in 1983–1984 imaged crust and upper mantle structure using a refraction survey and P-wave residuals from a 300 km seismic transect across the northern section of the CVL and the neighboring Adamawa Plateau. This study found evidence of a moderate LVA (approximately −2%) in the 100–200 km depth interval beneath the transect [*Dorbath et al*., 1986; *Plomerová et al*., 1993], as well as reduced crustal and lithospheric thickness beneath the Garoua Rift relative to the southern portion of the Adamawa Plateau [*Stuart et al*., 1985]. This finding was later confirmed by gravity studies [*Poudjom Djomani et al*., 1997, 1995].

Several more recent studies of crust and upper mantle seismic structure have been conducted using a 32 station broadband seismic experiment deployed across Cameroon from 2005 to 2007. *Tokam et al*. [2010] jointly inverted receiver functions and surface waves recorded on these stations to image crustal structure and found little evidence for crustal modification beneath the CVL. This conclusion was further supported by the results of a more recent H-k stacking analysis of receiver functions using the same data set [*Gallacher and Bastow*, 2012].

Reusch et al. [2010], using body wave tomography, imaged a uniform, vertically oriented, tabular low velocity zone directly below the CVL extending to at least 300 km depth. Using P-wave receiver functions to image the 410 and 660 km discontinuities, *Reusch et al*. [2011] showed that the transition zone beneath the CVL has not been thinned, indicating that the tabular LVZ in the upper mantle does not extend as deep as the transition zone.

Three recent studies have investigated shear wave splitting in the region of the CVL, finding broadly similar results but differing interpretations. *Koch et al*. [2012] calculated station-averaged shear wave splitting measurements and found that the fast direction beneath the CVL was variable but generally oriented N-S. Fast directions in the Congo Craton were NE-SW, while fast directions in the mobile belts between the CVL and the Congo Craton were ENE-WSW, consistent with direction of shear for the CASZ. A more recent study by *Elsheikh et al*. [2014] calculated shear wave splitting for individual event-station pairs and included additional stations. They found greater scatter in fast direction orientation beneath the CVL, with event-station pairs in the SW CVL showing a N-S orientation and pairs in the east and SE showing a NE-SW orientation, which *Elsheikh et al*. [2014] attribute to flow along a lithospheric channel created due to plate motion. A third study of SKS splitting using data from the stations deployed from 2005 to 2007 found evidence of similar NE-SW oriented fast direction near the southeastern boundary of the CVL, with null results in the southwest near the coast [*De Plaen et al*., 2014]. The authors interpreted the NE-SW splitting in the southeastern CVL as fossilized lithospheric anisotropy from the formation of the CASZ and suggested that the

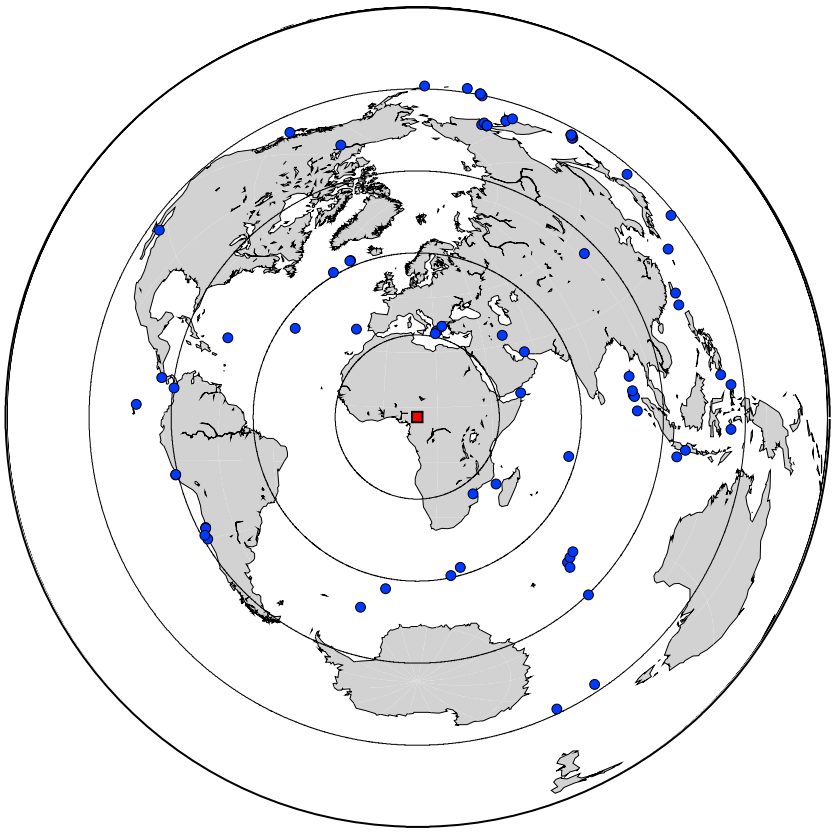

Figure 2. Map showing the location of all earthquakes used in this study as blue dots. Black concentric circles indicate distances intervals of 30° from the center of the array (red square).

null results near the coast may indicate replacement of the lithosphere in a process generating weak or unaligned anisotropy.

In all three studies of SKS splitting, the NE-SW oriented anisotropy is more closely spatially correlated with the surficial expression of the NE-SW shear along the CASZ than with the CVL (see *Elsheikh et al*., 2014, Figure 6; *De Plaen et al*., 2014, Figure 5), calling into question whether these locations represent the average structure of the CVL as suggested by *Elsheikh et al*. [2014] or fossilized anisotropy from the CASZ as suggested by *De Plaen et al*. [2014]. Furthermore, stations in the northernmost part of the study area in *Elsheikh et al*. [2014] are considered as part of the CVL, although these stations are up to 200 km away from surficial expression of the CVL. If these distant station event pairs and anisotropy spatially associated with the CASZ are eliminated, only a few stations in the CVL display NE-SW oriented anisotropy. In this study and in *Koch et al*. [2012], data in regions more closely associated with the CASZ are not included in analysis of the CVL to avoid contamination by the strong anisotropy expected for a major shear lineament.

3. Data and Methodology

3.1. Data set

We use data from a temporary passive seismic deployment installed across Cameroon from January 2005 through early 2007 [e.g., *Tibi et al*., 2005; *Reusch et al*., 2010, 2011; *Tokam et al*., 2010; *Koch et al*., 2012]. Eight broadband stations were installed in 2005 and operated for two years, and an additional 24 stations were installed in early 2006 and ran for a single year (Figure 1). Seismograms for events with $Ms > 5.5$ at epicentral distances from 30° to approximately 120° were chosen for visual inspection. From this initial set, events that were clearly recorded by at least five stations in this deployment and had a high signal-to-noise ratio were selected to be included in the inversion for phase velocities. The final data set includes a total of 87 events with a broad range of azimuthal distribution (Figure 2).

Table 1. Periods Studied and Corner Frequencies Used for Filtering Waveforms

Center Period (s)	Corner Frequencies (Hz)	
20.3051	0.0443	0.0542
22.3356	0.0403	0.0492
24.5692	0.0366	0.0448
27.0261	0.0333	0.0407
29.7287	0.0303	0.0370
32.7016	0.0275	0.0336
35.9718	0.0250	0.0306
39.5689	0.0227	0.0278
43.5258	0.0207	0.0253
47.8784	0.0188	0.0230
52.6663	0.0171	0.0209
57.9329	0.0155	0.0190
63.7262	0.0141	0.0173
70.0988	0.0128	0.0157
77.1087	0.0117	0.0143
84.8195	0.0106	0.0130
93.3015	0.0096	0.0118
102.6316	0.0088	0.0107
112.8948	0.0080	0.0097
124.1843	0.0072	0.0089
136.6027	0.0066	0.0081
150.2630	0.0060	0.0073
165.2893	0.0054	0.0067
181.8182	0.0049	0.0060

Seismograms were filtered and windowed for 24 periods ranging from 20 to 182 s. At each period, a zero-phase bandpass filter centered at each frequency was used to filter the seismograms (Table 1). For each event, window length was allowed to vary by period and was selected such that it contained the primary Rayleigh wave arrival at all stations while minimizing the inclusion of other phases. Events were further checked for quality at each period. Filtered and windowed seismograms at each period are shown in the online supplement for a sample event-station pair. If an event was not well recorded across a range of periods (usually at either high or low frequencies), that event was not included for inversion at those periods. For each filtered and windowed seismogram, phase and amplitude were measured using discrete Fourier analysis.

3.2. Phase Velocity Inversion

Traditional surface wave tomography methods represent a surface wave by a single plane wave propagating along a great-circle path from an earthquake to a receiver. This approximation is appropriate for small regions and for a spherically symmetrical Earth, but neglects the distortions of the wavefield created by heterogeneities along the travel path. Other approximations have been developed to circumvent this problem but involve greater numbers of unknowns. For example, *Friederich and Wielandt* [1995] represent the wavefield from a given event as a series of Hermite-Gaussian functions. This approach, however, requires large numbers of parameters to describe the wavefield and can create artifacts within the resulting velocity model. This study employs a method developed by *Forsyth and Li* [2005] in which the incoming wave field is approximated by the interference of two plane waves. This approach better accounts for heterogeneities along the travel path outside of the study area than traditional plane wave methods but does not require the solution of many unknowns as is the case for the *Friederich and Wielandt* [1995] method.

Following the method developed by *Forsyth and Li* [2005], we solve for phase velocities in two steps. First, an iterative simulated downhill simplex annealing method [*Press et al*., 1992] is used to solve for the phase, amplitude, and propagation azimuth of the two waves, while velocity is constrained to a constant initial velocity model. A secondary linearized inversion [*Tarantola and Valette*, 1982] is then used to solve for corrections to the initial velocity model while simultaneously further refining wave parameters by minimizing misfit to observations in a least-squares sense.

Inversions were conducted at each period for both one-dimensional and two-dimensional phase velocity structure. For one-dimensional inversions, Gaussian sensitivity to off-path structure was assumed. Using an initial uniform starting velocity of 4.0 km/s, we first solved for the average phase velocity at each period across the entire study region. This average phase velocity dispersion curve was used as a starting model for a second one-dimensional inversion in which the study region was split into three geologic regions as shown in Figure 3. For this second inversion, we solved for the average phase velocity for each period within each of these regions.

For the two-dimensional inversions, the phase velocity curves for each region were initially used as starting models to invert for phase velocities at each node. By refining the starting model used in each inversion, we sought to limit errors that might be introduced into the two-dimensional phase velocity maps by relying on a starting model that contains a priori information. Subsequent tests, however, indicated that the two-dimensional inversions had very limited sensitivity to the starting model. Therefore, the final phase

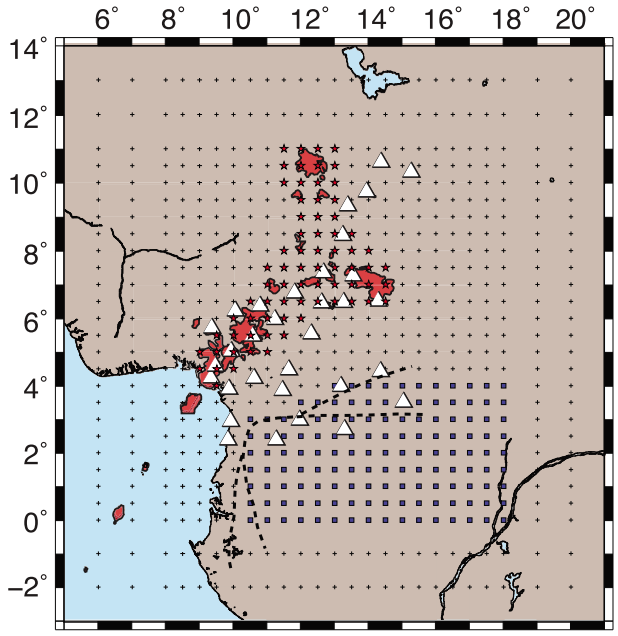

Figure 3. Location of nodes used in the inversion. Outer nodes are spaced 1 degree apart, while inner nodes are spaced at half degree intervals. Nodes associated with the CVL are shown as red stars, and blue squares indicate nodes associated with the Congo Craton. All other nodes are indicated by black crosses and are grouped together to show the structure of the geologic background. For reference, stations are shown in the background by white triangles.

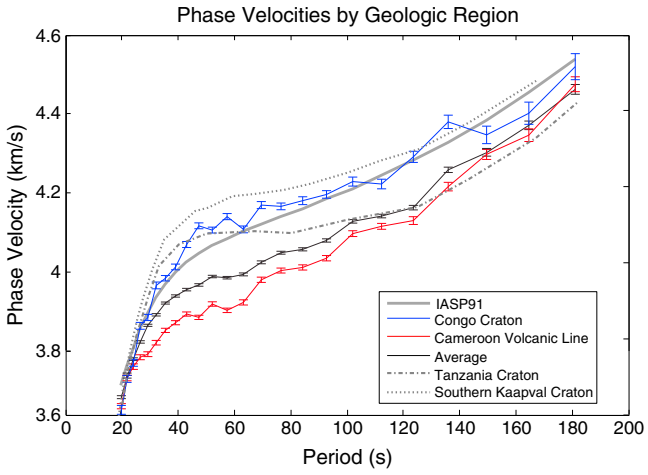

Figure 4. One-dimensional phase velocities determined for each region shown in Figure 3, with one-sigma standard deviations. Results from the Congo Craton are shown in blue, and results from the CVL are shown in red. The solution for a one-dimensional model that best fits the entire region is shown in black. For comparison, phase velocities for the IASP91 velocity model are shown by a bold gray line and phase velocities for other Archean African cratons are shown in light gray lines. Phase velocities for the Tanzania Craton [*Adams et al.*, 2012] are shown by a dash-dotted line, while velocities for the southern Kaapvaal Craton [*Adams and Nyblade*, 2011] are shown by a dotted line.

velocity maps presented in Figure 5 use the average one-dimensional phase velocity model for the entire study area as a starting model.

For average dispersion curves of the study region or individual geologic regions, the sensitivity of a Rayleigh wave to structure away from an idealized great-circle raypath is represented by a Gaussian sensitivity function with a characteristic length of 100 km. This approximation, however, does not accurately represent the sensitivity of a wave to structures that are on the order of its wavelength. To more accurately represent this off-path sensitivity and better resolve detailed structure, we use finite frequency sensitivity kernels in our two-dimensional inversions. *Zhou et al.* [2004] demonstrated the calculation of finite frequency sensitivity kernels for phase and amplitudes of surface waves along the travel path from source to receiver. They showed that the amplitude of sensitivity of surface wave is not constant with distance along the travel path and that the sensitivity of surface waves to off-path structure varies away from the assumed great-circle travel path with a pattern of alternating positive and negative polarity. The sensitivity kernels of *Zhou et al.* [2004] for full travel paths were applied to regional surface wave tomography, using both one and two plane waves, in a study by *Yang and Forsyth* [2006], which demonstrated that there is improved resolution of small features at periods above 50 s when the finite frequency effects of surface wave propagation are accounted for in this way.

The study area was divided into a set of exterior nodes with a spacing of 1° and covering an aperture of 14° by 15°, and more densely spaced interior nodes spanning an area of 10° by 11° with a spacing of 0.5°, totaling to 675 nodes (Figure 3). Dampening during the inversion was determined by an a priori error estimate assigned to each

Table 2. Initial Shear Wave Crustal Models

Region	Crustal Thickness	Vs at Depths <20 km (km/s)	Vs at Depths >20 km (km/s)	Vs in Uppermost Mantle (km/s)
CVL	34	3.50	3.89	4.45
Congo Craton	45	3.62	4.07	4.58
Benue Trough	26	3.34	3.73	4.33
Other Regions	36	3.60	3.90	4.45

node. A higher error estimate was assigned to exterior nodes (1.5 km/s) relative to interior nodes (0.15 km/s) to allow the exterior nodes, which are outside of our primary areas of interest, to preferentially absorb any abnormalities in the incoming wavefield that could not be accounted for by using the two-plane wave approximation. For the two-dimensional inversion, which also includes a solution for average anisotropy within each geologic region for each period, we also assigned an a priori error estimate of 0.03 km/s to anisotropic parameters.

3.3. Shear Velocity Inversion

To analyze shear wave velocity structure for our study area, we calculate a three-dimensional shear wave velocity model. Radial shear wave velocity profiles are calculated using a linearized inversion [*Herrmann and Ammon*, 2002] to solve for the best-fitting shear wave velocity in a least-squares sense at each of the interior nodes in the study area (Figure 3). The one-dimensional shear wave velocity profiles are laterally smoothed with the same 100 km Gaussian smoothing algorithm used for the phase velocity inversion and are interpolated to a lateral spacing of 0.1° and a vertical spacing of 10 km to create a quasi three-dimensional model. Several inversion schemes were tested including inversion in a flat-earth parameterization using the codes of *Herrmann and Ammon* [2002] and *Julia et al*. [2000] and the spherical parameterization of *Saito* [1981]. All codes gave similar structure within the upper 200 km, where the data have the best resolution.

The Rayleigh wave eigenfunctions at periods used in this study are sensitive to but have limited ability to resolve structure at crustal depths. To account for this, we used realistic starting crustal velocity models from *Tokam et al*. [2010] for all continental crustal nodes (Table 2), which were calculated from the joint inversion of group velocities and receiver functions. Crustal velocities and layer thicknesses for oceanic nodes were from the Crust2.0 model [*Bassin et al*., 2000]. Mantle velocities in all starting models were spherical Earth velocities from IASP91 [*Kennett and Engdahl*, 1991], with 10 km thick layers to a depth of 1130 km, underlain by a halfspace. P-wave velocities for the starting model were calculated using a Vp/Vs ratio of 1.73, and densities from AK135 were used [*Kennett et al*., 1995]. Velocities for depths greater than 410 km, where our phase velocities have very little sensitivity, are fixed to the initial model. Vertical smoothing across all layers, except across the Moho, was included in the inversion. An initial two inversions were run with a high damping parameter of 10, followed by an additional 50 iterations with a damping parameter of 0.05.

One of the limitations of this methodology is the inability to quantify uncertainties in the shear wave velocity model. To address this issue, we also perform a Markov chain Monte Carlo simulation [*Shapiro and Ritzwoller*, 2002; *Heeszel et al*., 2013] to explore the range of shear wave models for the average structure of the CVL and the Congo Craton that may match our phase velocity results. In the linearized quasi three-dimensional inversion, layer thickness is fixed. Using the Monte Carlo simulation, however, layer thickness in the crust is allowed to vary to test the effects of crustal structure, which is not well resolved, on the upper mantle velocity model. Crustal thickness is allowed to vary by up to 5 km. Velocities are allowed to vary by different percentages depending on depth. Velocities are allowed to vary by 10% in the upper 210 km and by 2% from 210 to 410 km. Velocities at depths greater than 410 are not allowed to vary due to the very limited resolution that our data provide at these depths. In our linearized inversion for shear wave velocity structure, we solve for spherical Earth velocities, while the Monte Carlo simulation is performed for flat-earth velocities. For the initial model used in the Monte Carlo simulation, we use our best-fit solution from the linearized inversion, with a standard earth-flattening transform applied [*Aki and Richards*, 2002].

4. Results

4.1. Phase Velocities

A one-dimensional average phase velocity dispersion curve for the entire study region is shown in Figure 4, together with average phase velocities separated by geologic region as illustrated in Figure 3 and the phase velocities predicted for the global model IASP91. Values and one standard deviation uncertainties for

Table 3. Phase Velocity Results

	Average		Regional Background		Congo Craton		CVL	
Period (s)	Velocity	Std. Dev.	Velocity	Std. Dev.	Velocity	Std. Dev.	Velocity	Std. Dev.
20	3.649	0.004	3.676	0.005	3.615	0.012	3.625	0.007
22	3.702	0.003	3.706	0.005	3.697	0.009	3.699	0.007
25	3.749	0.003	3.760	0.005	3.738	0.009	3.729	0.007
27	3.794	0.003	3.813	0.005	3.836	0.009	3.754	0.006
30	3.838	0.003	3.883	0.004	3.858	0.008	3.762	0.006
33	3.865	0.003	3.899	0.005	3.942	0.009	3.792	0.006
36	3.896	0.003	3.930	0.004	3.961	0.007	3.824	0.005
40	3.915	0.003	3.948	0.004	3.991	0.008	3.844	0.005
44	3.931	0.003	3.952	0.005	4.050	0.008	3.867	0.005
48	3.944	0.003	3.976	0.004	4.099	0.008	3.858	0.006
53	3.966	0.003	3.997	0.005	4.088	0.008	3.894	0.006
58	3.963	0.003	3.991	0.005	4.123	0.008	3.877	0.006
64	3.971	0.004	3.991	0.005	4.090	0.009	3.898	0.007
70	4.003	0.004	3.992	0.005	4.154	0.009	3.957	0.007
77	4.028	0.004	4.033	0.005	4.150	0.009	3.981	0.007
85	4.037	0.004	4.044	0.006	4.165	0.010	3.990	0.007
93	4.061	0.004	4.067	0.006	4.182	0.010	4.014	0.007
103	4.111	0.005	4.106	0.006	4.215	0.012	4.079	0.008
113	4.125	0.005	4.132	0.007	4.209	0.013	4.098	0.008
124	4.147	0.006	4.155	0.008	4.280	0.015	4.113	0.010
137	4.246	0.007	4.256	0.010	4.372	0.017	4.202	0.011
150	4.291	0.009	4.290	0.012	4.338	0.023	4.287	0.013
167	4.363	0.011	4.358	0.015	4.395	0.029	4.337	0.017
182	4.458	0.013	4.456	0.017	4.518	0.034	4.471	0.020

these phase velocity curves are shown in Table 3. Formal standard deviations from model parameters calculated using this methodology are frequently very small [e.g., *Weeraratne et al*., 2003; *Adams et al*., 2012; *O'Donnell et al*., 2013]. Therefore, for estimates on uncertainty that are likely more realistic, we refer the reader to the two sigma error estimates of our two-dimensional models (Figure 5).

The Congo Craton is faster than the Cameroon Volcanic Line at all periods, a difference that is most pronounced at periods between 24 and 143 s, and becomes smaller at the longest periods included in this study. Similarly, the CVL is slower than the velocity of the regional background, most notably at periods between 22 and 64 s. The greater difference in velocity between the CVL and the Congo Craton and background regions at shorter and moderate periods is an indication that low velocities beneath the CVL are likely concentrated at shallow depths within the mantle. At periods less than 43 s, phase velocities for the regional background are comparable to those for the Congo Craton, indicating that crustal velocities are similar for the Congo Craton and the surrounding region. This finding is consistent with previous studies finding similar crustal shear wave velocity structure for the Craton and the CASZ [e.g., *Tokam et al*., 2010].

Figure 4 also shows phase velocities measured for the Tanzania Craton [*Adams et al*., 2012] and the Kaapvaal Craton [*Adams and Nyblade*, 2011]. At periods shorter than 50 s, the Congo Craton is slower than both the Tanzania and the southern Kaapvaal Craton, which likely indicates a difference in crustal structure, possibly influenced by the sedimentary cover along the edges of the Craton. At longer periods, however, average phase velocities for the Congo Craton are faster than those associated with the Tanzania Craton, where there is evidence for a large-scale upper mantle velocity anomaly [*Adams et al*., 2012], but slower than those for the southern Kaapvaal Craton, where there is no evidence for perturbation of the sublithospheric mantle [*Adams and Nyblade*, 2011].

Figure 5 shows phase velocity maps from the two-dimensional phase velocity inversions for selected periods. Recovered checkerboards calculated from the resolution matrices for similar periods are shown in Figure 6. Maps in both figures have been clipped to show only those areas with a standard deviation of 0.08 km/s or less. Inversions also include a solution for azimuthal anisotropy within each geologic region (discussed in more detail in section 4.2).

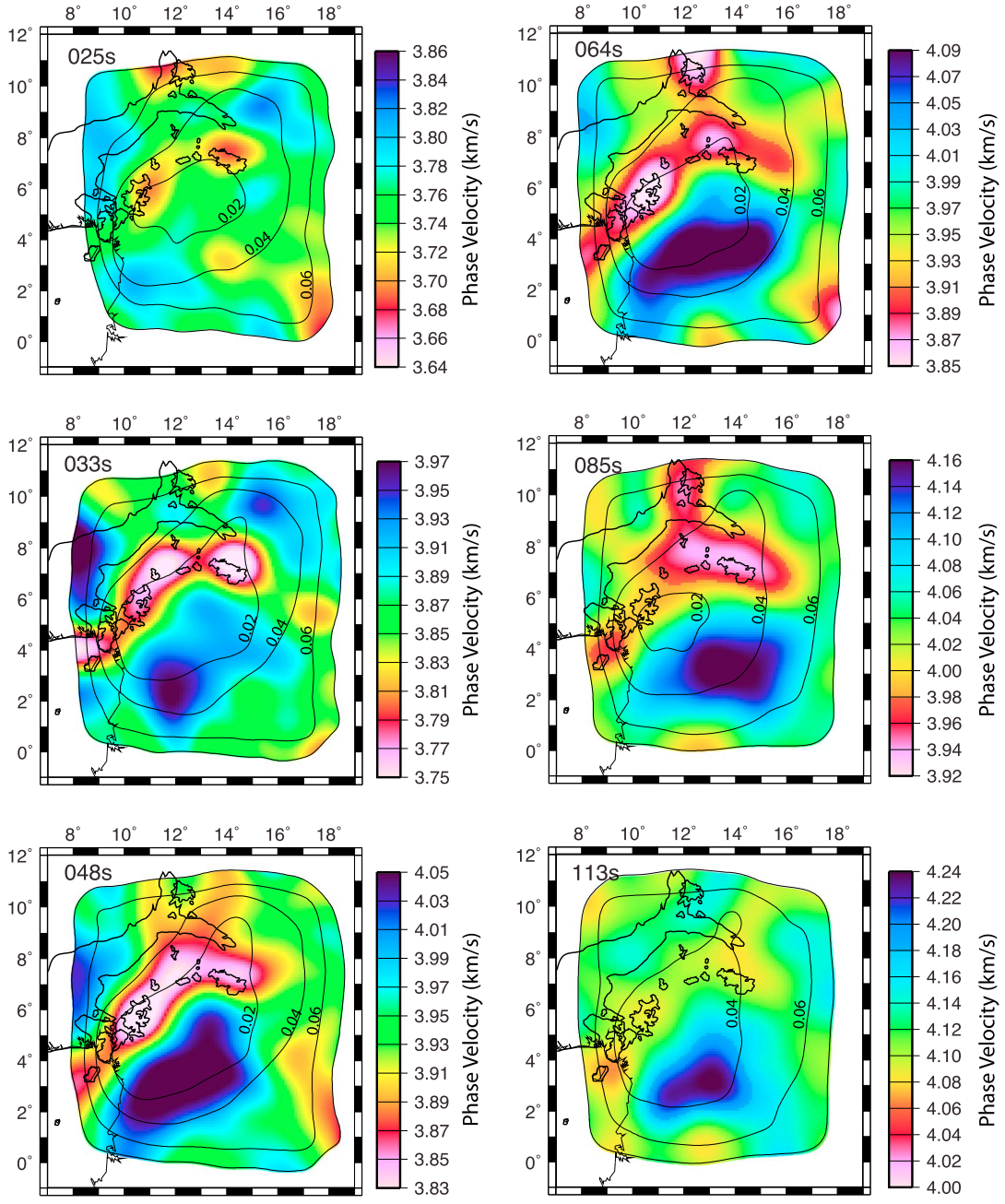

Figure 5. Phase velocity maps for selected periods. The color scale for each period covers +/−3% of the average phase velocity for that period. Maps are clipped to show only those regions where the 2-sigma standard deviation is less than 0.08 km/s, and contours show areas with standard deviation less than 0.06, 0.04, and 0.04 km/s.

At periods of 25 s and less, velocities beneath the CVL are slower, on average, than for surrounding regions, but the velocity anomalies are spatially isolated and are not coherent from one period to another. At these short periods, slow and fast velocity anomalies are dispersed throughout the study region, likely indicating local variations in crustal structure, composition, and sediment thicknesses. Resolution tests indicate that the locations of these anomalies are well resolved to 2° in the center portion of our study region but that lateral smearing may distort the locations in the northwestern and southeastern portions of the model.

At periods of 27 s and greater, a continuous pattern of low velocity is found beneath the CVL. Between 27 and 48 s, low velocities are found beneath the southwestern CVL and the eastern branch of the CVL, but no similar

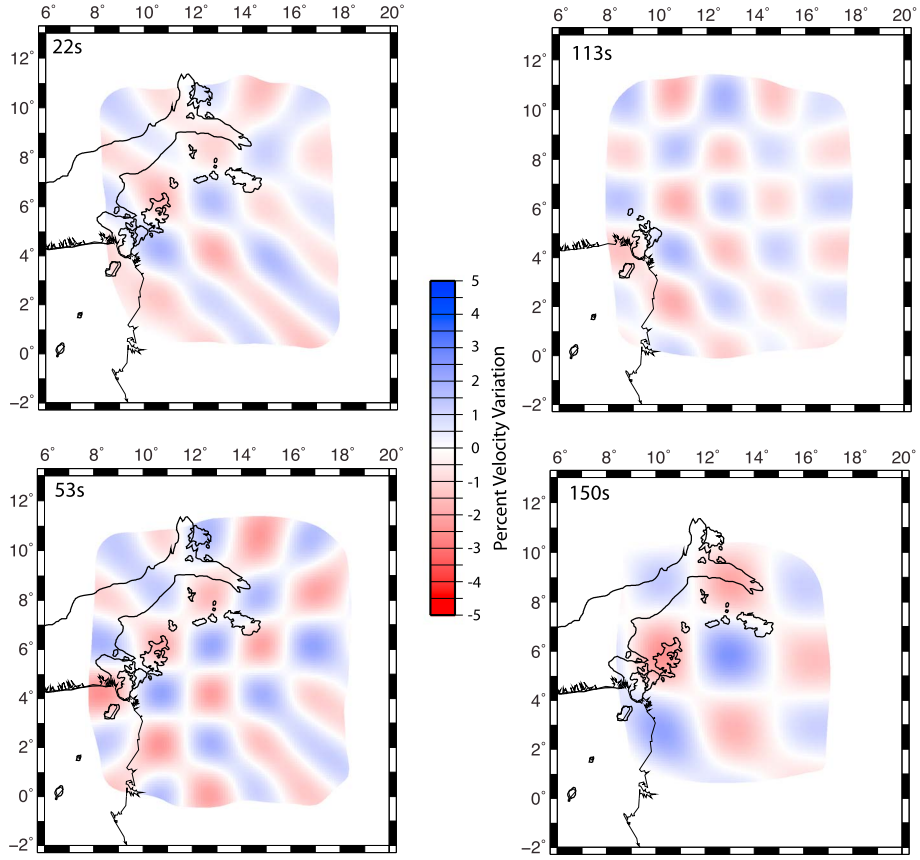

Figure 6. Maps of a recovered checkerboard pattern of velocity anomalies calculated using the resolution matrix. Input checkers were 2° squares alternating +/−5% velocity variation for periods less than 150 s. For periods of 150 s and greater, 2° squares were not well resolved and results for 3° checkers alternating +/−5% velocity variation are shown. Recovered checkers for additional periods are shown in the online supplement.

pattern of low velocity is found beneath the northern CVL. Low velocities extend to the northern branch at periods of 53 s and greater, although at all periods, phase velocity is more reduced beneath the southern and eastern branches of the CVL than beneath the northern branch.

At periods of 27 s and greater, a strong fast phase velocity anomaly is found beneath the northern Congo Craton. On the easternmost side of the Craton, velocities are reduced with respect to the northern Craton but are still fast relative to the CVL. These features are observed in other tomography models [e.g., *Ritsema and van Heijst*, 2000] and are most likely attributable to the Neoproterozoic rift structures of the Cuvette Centrale in the east and south [e.g., *Daly et al*., 1992]. However, resolution tests indicate that the precise shape and location of these slower regions may not be well resolved; thus, we do not offer a detailed interpretation of their internal structure.

Figure 6 shows the recovery of input checkerboard models for selected periods, calculated from the resolution matrix of the inversion with an input model of squares alternating plus and minus 5% velocity variation (additional periods are shown in the online supplement). For periods less than 150 s, 2° checkers are well resolved. Recovery of the input checkers is best in the central portion of the study region, where station and raypath density are greatest. At longer periods, 2° checkers are not well resolved, but 3° checkers can be recovered.

4.2. Phase Velocity Anisotropy

The magnitude and direction of the fast axis of azimuthal anisotropy at each period are shown in Figure 7 for the CVL, Congo Craton, and regional background as defined in Figure 3. At periods of 20 to 43 s, anisotropy within the CVL ranges from 1% to 2% and the fast axis is oriented roughly north-northeast. At periods greater

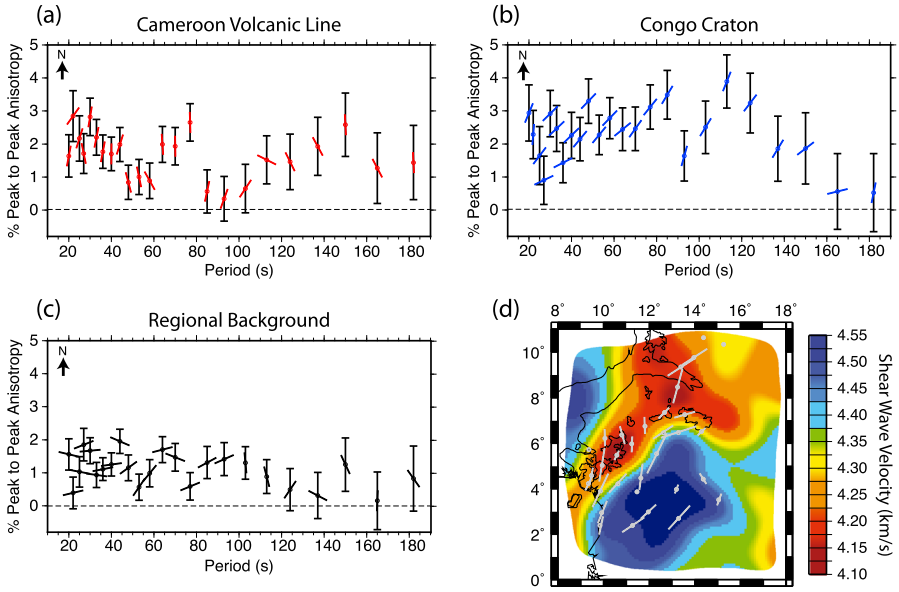

Figure 7. Average azimuthal anisotropy is shown for each set of nodes indicated in Figure 3, with (a) the CVL shown in red, (b) the Congo Craton shown in blue, and (c) the regional background shown in black. Each plot shows percent peak-to-peak anisotropy plotted against period. The direction of the line at each period relative to the north arrow indicates the orientation of the fast direction of propagation. For comparison with previous studies, Figure 7d shows shear wave splitting results from *Koch et al.* [2012] plotted over shear wave velocities at 100 km depth from this study.

than 43 s, anisotropy within the CVL varies significantly, both in terms of amplitude and azimuthal distribution, but is generally oriented N-S and is less than 3%. Anisotropy for the Congo Craton is consistently oriented northeast-southwest at all periods. With the exception of the two longest periods measured, anisotropy varies from 1% to 4%. Anisotropy within the regional background, including the Benue Trough and the CASZ, shows less pronounced anisotropy, with percent anisotropy limited to 2% or less at all periods. The azimuthal direction of the background anisotropy at periods greater than 100 s is scattered, but at shorter periods, the fast direction is oriented roughly E-W. This may represent the lithospheric deformation of the E-W oriented CASZ in the center of the study region, which is included as part of the regional background. These results are consistent with shear wave splitting results, which show a roughly N-S orientation of the fast propagation direction for the CVL and a NE-SW direction for much of the Congo Craton [*Koch et al.*, 2012] (see Figure 7). *Koch et al.* [2012] found predominantly E-W fast direction orientations for stations located within the CASZ.

4.3. Shear Wave Velocity Results

One-dimensional shear wave velocity profiles calculated from the average phase velocities of the CVL and the Congo are shown in Figure 8. The Congo Craton displays a thick lid, typical of an Archean craton, with a peak velocity of 4.62 km/s at a depth of 80 km. The lid structure reaches a depth of approximately 200 km, based on the depth of the velocity minimum and is comparable to global average velocities. In contrast, Figure 8 shows that the CVL is characterized by a pronounced low velocity zone between depths of 50–150 km and less pronounced low velocities extending to even greater depths. The results also show that the mantle lithospheric lid is either missing or very thin. The uppermost mantle velocities are highest at the Moho (4.39 km/s) but rapidly decrease within the upper 20 km of the mantle, with a velocity minimum of 4.22 km/s reached at a depth of 80 km.

Velocities were allowed to vary at depths up to 410 km; however, resolution at these depths is very limited, both due to depth sensitivity and lateral resolution. Phase velocities measured for periods used in this study have limited sensitivity to depths greater than 200 km. Furthermore, resolution tests indicate that lateral structure is less resolved at the longest period included in this study. Therefore, we do not interpret structures at depths greater than 200 km.

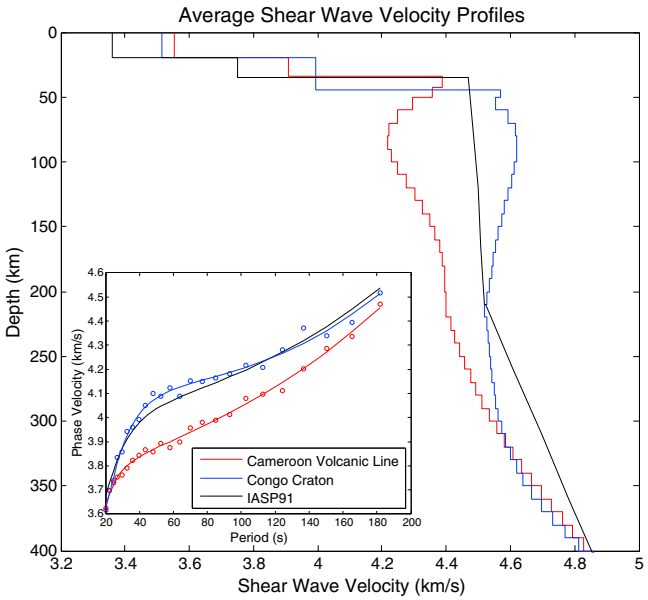

Figure 8. Average shear wave velocity profiles for the CVL and Congo Craton, shown with IASP91 for comparison. The inset shows the phase velocity measurements from which the average shear wave velocities were derived (symbols) and the phase velocities predicted by the best-fitting shear wave velocity model (lines).

Shear wave velocity maps at selected depths from our three-dimensional shear wave velocity model are shown in Figure 9, and Figure 10 shows cross-sectional views through the model as indicated in Figure 9c. Maps are clipped with the same mask used for the 53 s phase velocity maps. Figure 9a shows velocities at 50 km depth, where shallow low velocities are found beneath the southern and eastern branches of the CVL, while beneath the northern branch of the CVL, faster velocities extend to a depth of approximately 75 km. The fast lithosphere of the Congo Craton extends to depths of approximately 175 to 200 km, measured at the velocity minima beneath the central regions of the Craton.

Along the length of the CVL, there is limited lateral variation in velocity (Figure 10b), an observation that is inconsistent with localized magma sources at upper mantle depths along strike of the CVL. A sharp vertical transition from slow velocities beneath the CVL to fast velocities beneath the Congo Craton is observed at all depths in the model, although the difference in velocity is less pronounced at greater depths.

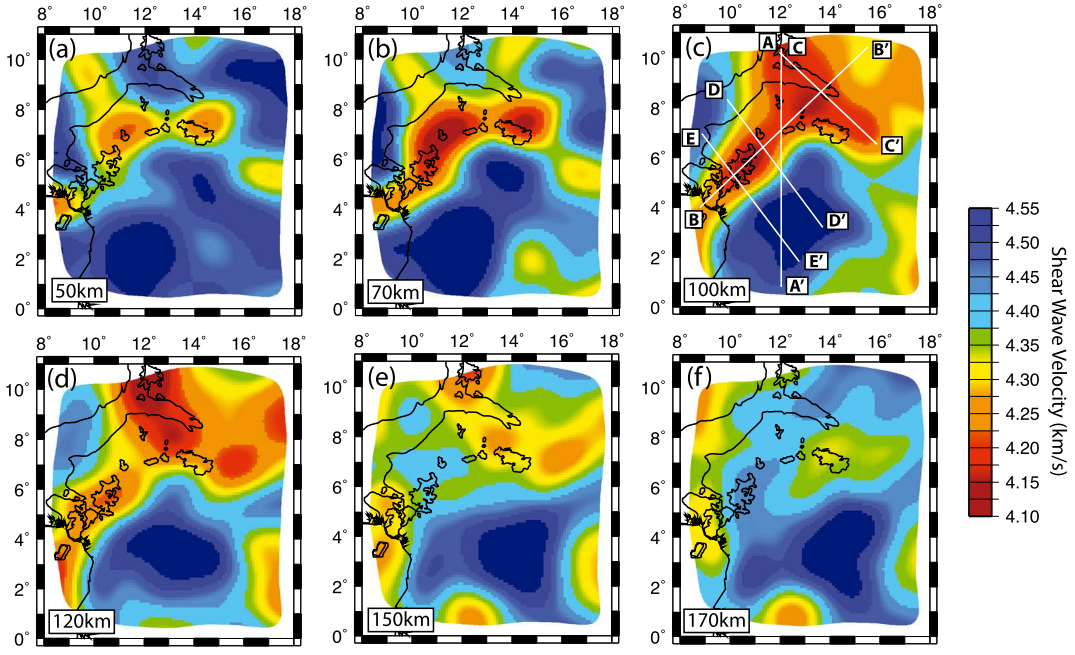

Figure 9. Selected depth slices through the shear wave velocity model. The maps are clipped using the clipping mask used to clip the 58 s phase velocity map.

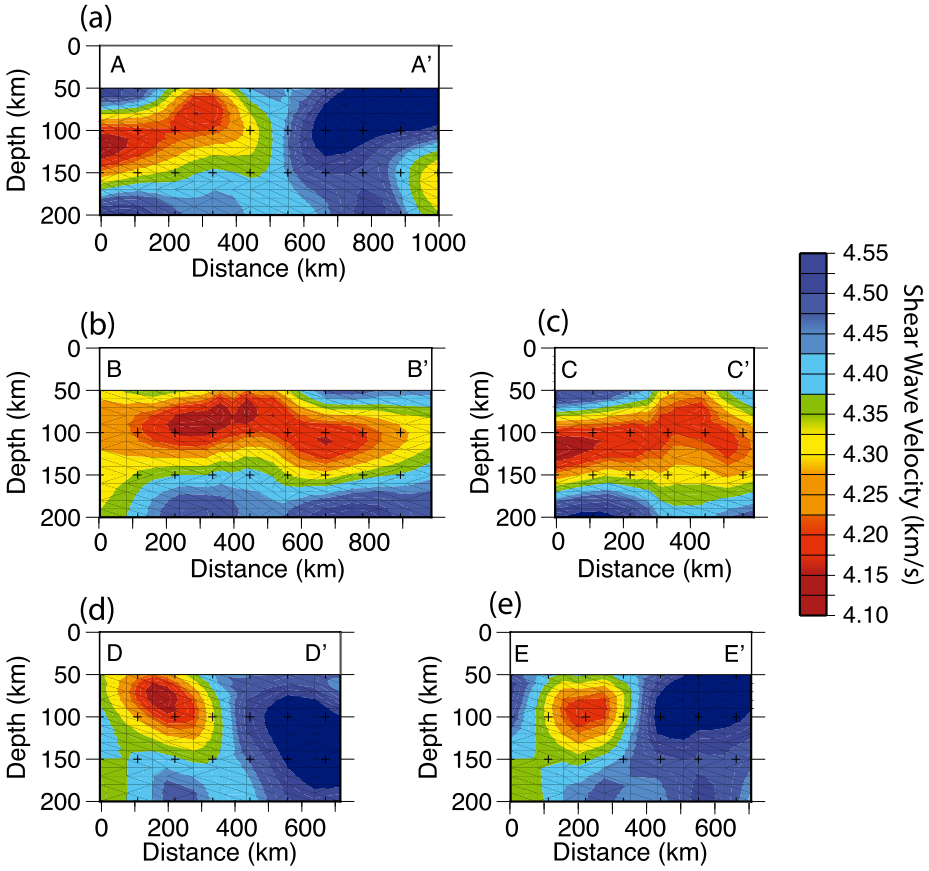

Figure 10. Cross sections through the shear wave velocity model. Crosses represent depth intervals of 50 km and lateral distance intervals of 1°. (a–e) Cross sections through different locations as illustrated.

Monte Carlo simulations testing perturbations to crustal thickness and crustal and mantle velocities from our best-fitting models from linearized inversion are shown in Figure 11. For both the CVL and the Congo Craton, the average model from Monte Carlo simulations is very similar to the model calculated from the linear inversion, and all acceptable models are evenly distributed around the model from the linear inversion. The

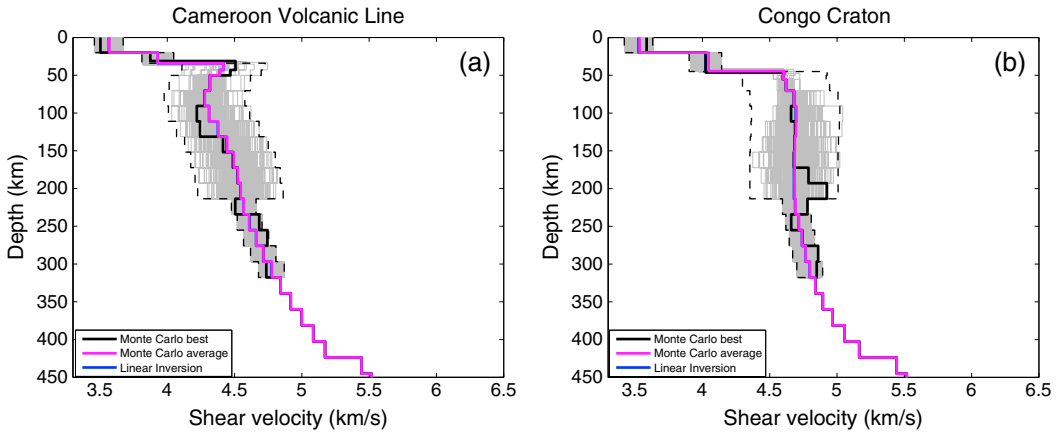

Figure 11. Monte Carlo simulations for (a) the CVL and (b) the Congo Craton. Best-fitting models from the linearized inversion are shown in blue. Models from the Monte Carlo simulation are shown as black thin gray lines, while the best-fitting model is shown in black and the average model is shown in magenta. Limits placed on acceptable models are shown by dashed lines.

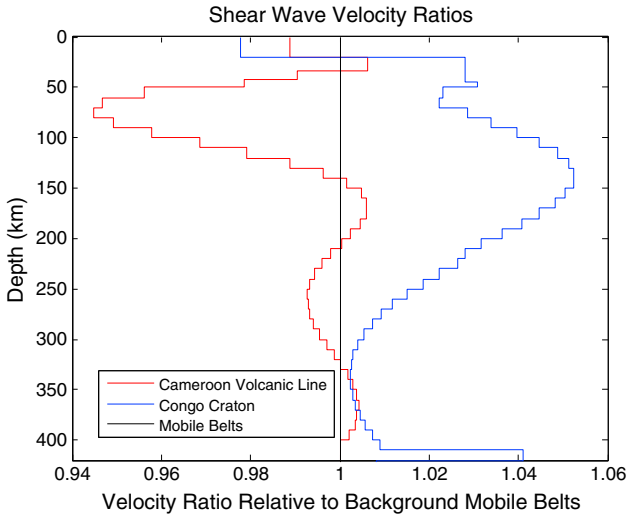

Figure 12. Ratios of the average shear wave velocity profiles for the CVL and the Congo Craton relative to average shear wave velocity of the background nodes (Figure 3), which primarily consist of Pan-African mobile belts.

strong velocity reduction in the uppermost mantle beneath the CVL is well resolved, as indicated by the decreased variability in models at depths between 50 and 100 km. For both the CVL and the Congo Craton, however, the best-fitting model from the Monte Carlo simulation displays greater oscillations than the average model or the linear model. This is most notable for the Congo Craton, where the large swings at depths between 110 and 220 km are probably unrealistic.

5. Discussion

5.1. Lithospheric Instability

The shear velocity structure derived from Rayleigh wave tomography shows a pronounced low velocity zone beneath the CVL at depths between 50 and 150 km, with the strongest velocity reduction of approximately −4% at depths between 70 and 120 km relative to the fastest velocities in the uppermost mantle. These slow velocities are separated from the fast velocities beneath the Congo Craton by a vertical boundary that extends to at least 200 km, although the velocity contrast across the boundary decreases with depth. These results, together with evidence from body wave [*Reusch et al*., 2010] and transition zone receiver function [*Reusch et al*., 2011] studies, create a clear model of a vertical low velocity zone beneath the CVL that extends from the base of the crust to depths between 200 and 300 km, but not into the upper mantle transition zone. These observations are used to evaluate candidate origin models for the formation of the CVL in section 5.2.

To further examine the alteration of the upper mantle of the CVL from the host rocks of the surrounding region, Figure 12 shows the ratio of average velocities beneath the CVL and the Congo Craton relative to the average background velocity, which primarily consists of Pan-African mobile belts into which the CVL was erupted. At all subcrustal depths, velocities beneath the CVL are slower than the background, showing no evidence for typically seismically fast lithospheric mantle beneath most of the CVL. Geochemical evidence from isotopic studies [*Déruelle et al*., 2007] and studies of mantle xenoliths [*Déruelle et al*., 1991; *Principalle et al*., 2000; *Déruelle et al*., 2007] indicate that CVL volcanics are sourced from the sublithospheric mantle. This geochemical evidence for sublithospheric melt, together with the slow velocities that extend to the base of the crust beneath the main branch of the CVL, indicates that the lithospheric mantle has likely been eroded or highly altered beneath the main branch of the CVL and has to a lesser extent been thinned beneath the northern branch of the CVL. The cross-section shown in Figure 10a clearly demonstrates the transition from a thinned lithosphere beneath the northern CVL, to the eroded lithosphere beneath the main branch of the CVL, to the thick, fast lithosphere beneath the Congo Craton.

5.2. Models for the Formation of the Cameroon Volcanic Line

Several models have been proposed for the formation of the CVL. Some models evoke single or multiple mantle plumes [*Ngako et al*., 2006], others suggest that pre-existing lithospheric structures control the formation of the CVL [*Ebinger and Sleep*, 1998], and a large class of proposed models rely on convection driven by various forces to form the CVL (Figure 13) [*King and Anderson*, 1995, 1998; *Meyers et al*., 1998; *King and Ritsema*, 2000]. Here we briefly describe these models and the implications that results from previous studies and this study have for their viability.

Many linear volcanic chains have formed by the progression of a plate moving across a hot spot. Although some studies have suggested this as a possible source for the CVL (Figure 13a) [e.g., *Morgan*, 1983; *Van Houten*, 1983; *Lee et al*., 1994; *Burke*, 2001], geochemical studies indicate a lack of age progression along the line, making this simple hot spot model an unlikely source for the CVL [e.g., *Hedberg*, 1969; *Grant et al*., 1972;

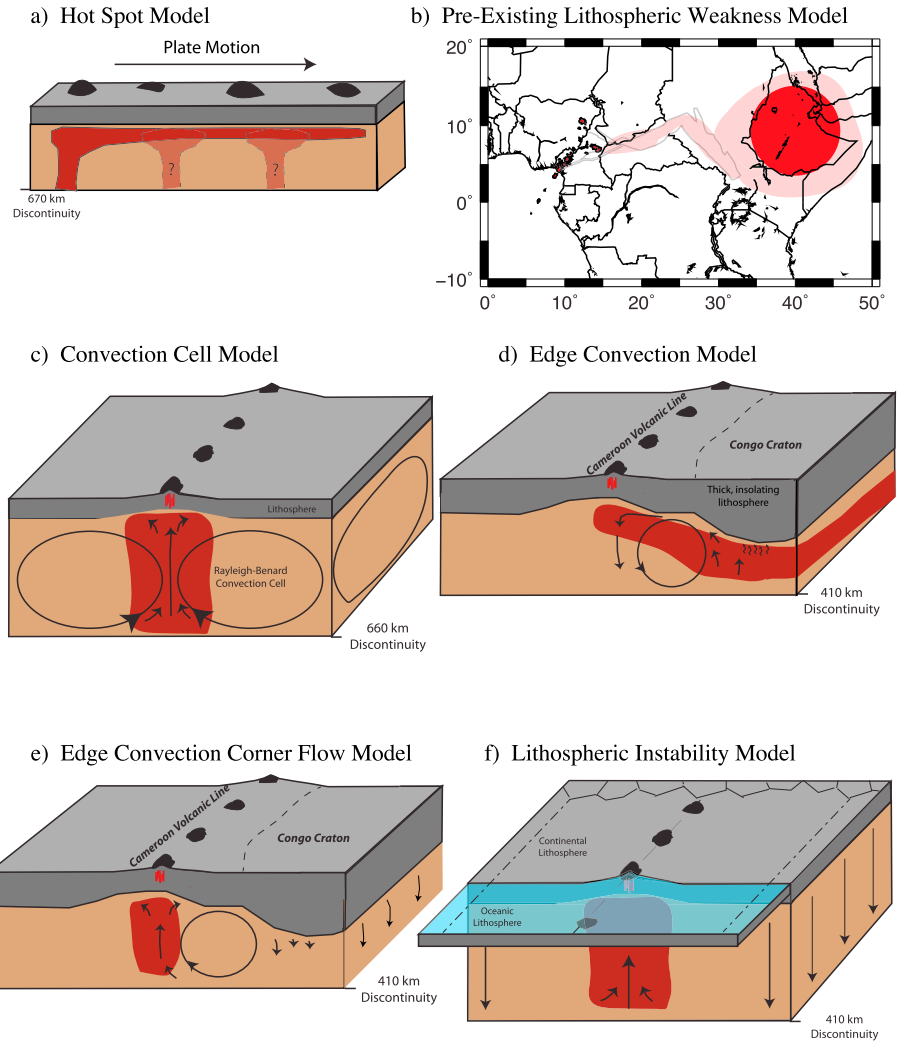

Figure 13. Potential geodynamic models for the formation of the CVL. (a) Hot spot or multiple hot spot model. (b) Pre-existing weakness model, with possible transport of material from the Afar hot spot [from *Reusch et al.*, 2010; after *Ebinger and Sleep*, 1998]. (c) Rayleigh-Baynard convection cell model [after *Meyers et al.*, 1998]. (d) Edge convection model with lateral flow of warm material from beneath the Congo Craton [*King and Anderson*, 1995]. (e) Corner-flow eddy model [*King and Anderson*, 1998; *King and Ritsema*, 2000]. (f) Lithospheric instability along continental margin [*Milelli et al.*, 2012].

Grunau et al., 1975; *Dunlop and Fitton*, 1979; *Cornen and Maury*, 1980; *Dunlop*, 1983; *Fitton and Dunlop*, 1985; *Lee et al.*, 1994; *Ngounouno et al.*, 1997; *Marzoli et al.*, 1999, 2000; *Ngounouno et al.*, 2001, 2003; *Njilah et al.*, 2004; *Ngounouno et al.*, 2005, 2006; *Aka et al.*, 2009; *Dongmo et al.*, 2010; *Kamgang et al.*, 2010]. Other plume-based models have been proposed, however, including multiple plumes impinging on the lithosphere, with volcanics from one hot spot track overprinting the linear age progression created by another [*Ngako et al.*, 2006].

Tomographic results, however, do not show support for either a single plume or multiple plumes as the source of the CVL. In this study, no localized areas of slower velocities along the CVL delineating separate plumes are observed, particularly at depths of around 100 km where the largest anomalies are found (Figure 9c). Body wave tomography has shown a similar lack of localized low velocity regions [*Reusch et al.*, 2010]. Anisotropy results also do not support the presence of a mantle plume or plumes in this location, which may be expected to exhibit a radial pattern of anisotropy around the conduit [*Weeraratne et al.*, 2003; *Montelli et al.*, 2004; *Behn et al.*, 2004; *Farnetani and Samuel*, 2005] or rings in which the fast direction is oriented tangential to radial flow [*Druken et al.*, 2013]. *Koch et al.* [2012] found no evidence for either pattern in their study, which provided constraints on the lateral variations in the fast propagation direction. Our study

does not provide strong constraints on lateral variation in anisotropy but does indicate that each region has a dominant fast propagation direction that is consistent across multiple periods. This observation would be unlikely if the direction of fast propagation was changing rapidly within a given region, as would be expected for a mantle plume.

Other studies have suggested that the CVL was created by the diversion of material from a distant plume along pre-existing weaknesses in the lithosphere. The most prominent of these models is the suggested diversion of hot mantle material from the Afar plume in East Africa through the CASZ to the CVL (Figure 13b) [*Ebinger and Sleep*, 1998]. This process, however, should create an age progression from older volcanics in the east to younger volcanics in the west, which is not observed. Furthermore, the N-S orientation of the fast direction of propagation found in this study and by *Koch et al*. [2012] is at large angles to the expected flow direction and the predicted direction of anisotropy for such a model, and thus does not support flow along strike of the CVL.

The first of several convection-based models for the origin of the CVL proposes that shear in the mantle transition zone drives upper mantle convection cells (Figure 13c). *Meyers et al*. [1998] proposed a model in which shear heating and heat transfer along the 660 km discontinuity at the base of the transition zone, with limited shear at the base of the lithosphere, generate a series of Rayleigh-Baynard convection cells on the scale of 1000 km, with alternating convective directions. *Meyers et al*. [1998] suggest that the CVL may represent the convergence of upwelling limbs from two such convection cells. Frictional heating due to shear and heat transfer at the base of the transition zone would create a thermal anomaly at depth which would then form the base of an upwelling limb of the convection cell. Evidence has been found for similar, but shallower, convection cells have been found beneath linear volcanic chains without age progression west of the East Pacific Rise [*Harmon et al*., 2011]. *Harmon et al*. [2011] found evidence that these convection cells were associated with both partial melt and a thermal anomaly. In this study, we observe a low velocity zone that is pronounced down to 200 km depth. Although there is evidence that the deviation from regional and global average velocities decreases at greater depths, resolution at these depths is limited. Previous studies with resolution deeper in the upper mantle [*Reusch et al*., 2010] have found that low velocities beneath the CVL extend only to depths of 300–400 km and found no evidence for deflection in the depths of major mineral phase changes in the transition zone [*Reusch et al*., 2011], making such large-scale Rayleigh-Baynard convection cells an unlikely geodynamic source for the CVL.

Another possible mechanism for the formation of the CVL is convection influenced by the neighboring Congo Craton, of which two variations have been suggested. *King and Anderson* [1995] suggest that the juxtaposition of the insolating lithosphere of an Archean craton such as the Congo Craton and the thinner lithosphere of a younger terrain such as the region north of the Congo Craton creates a contrast in heat flux which should drive warm material beneath the craton to flow laterally and upward beneath the CVL. Seismically, this would be expressed as a low velocity zone confined to shallow depths directly beneath the CVL, dipping toward the Congo Craton with increasing depth (Figure 13d). This model is not supported by results from previous body wave tomography study [*Reusch et al*., 2010] or by results from this study, which both find evidence for a strong vertical boundary between fast velocities beneath the Congo Craton and slow velocities beneath the CVL. Furthermore, these studies find that low velocities beneath the CVL extend to depths of at least 300 and 200 km, respectively, which does not support the shallow anomaly expected for this mechanism.

A more recent edge convection numerical model suggests that a corner-flow eddy in the upper mantle created at boundary of two terrains with significantly different lithospheric thicknesses would be stronger than the thermally driven flow described by *King and Anderson* [1995] in the absence of a large positive thermal anomaly beneath the thicker lithosphere [*King and Anderson*, 1998; *King and Ritsema*, 2000]. In this model, a downwelling would form at the edge of thick, cold lithosphere due to cooling and sinking of the surrounding mantle, while an upwelling would form beneath an adjacent terrain with thinner lithosphere. *Reusch et al*. [2010] suggest this mechanism as a source for the CVL, with an edge convection-driven downwelling at the edge of the Congo Craton and an associated upwelling beneath the CVL (Figure 13e). In this study, we find evidence for a linear low velocity region directly beneath the CVL, with fast velocities at all depths beneath the Congo Craton, and that boundary between these two regions is vertical. These findings are consistent with those from body wave tomography [*Reusch et al*., 2010] and match the seismic

pattern expected for a corner-flow eddy. It is important to note, however, that the western edge of the Congo Craton, which might drive this mechanism for the offshore CVL, is not well defined. It may follow the coast of the continent, running subparallel to much of the oceanic CVL, or it may turn away from the coast, diverging from the oceanic CVL. Given this uncertainty of the proximity of the western edge of the Congo Craton to the oceanic CVL, it is unclear whether edge convection alone could have created the oceanic CVL without interaction with another dynamic process such as diversion of material along pre-existing offshore structures or a geographically coincident offshore mantle plume.

A recent study by *Milelli et al*. [2012] used laboratory experiments of viscous fluids to model convection induced by instabilities from lithospheric cooling at the boundaries of continents, where the thick viscous continental lithosphere is surrounded by the less viscous asthenosphere beneath thin oceanic lithosphere. Their experiments show that hexagonal convection cells beneath continental interiors give way to linear upwellings and downwellings near continental margins, which destabilize and destroy the lower part of the lithosphere. In their experiments, these linear features developed perpendicular to the continental margin, extending both onshore and offshore, and often displayed branching patterns (Figure 13f). *Milelli et al*. [2012] report that the length scale of the CVL is comparable to the length predicted by their model for a radial upwelling along the boundary of a circular continent with a radius similar to that of Africa. This model shares similar features with that of *King and Anderson* [1998], but the driving mechanism is differential cooling of the lithosphere along the ocean-continent margin. This will produce an upwelling perpendicular to ocean-continent boundary, in contrast to an edge-flow eddy that would produce upwelling parallel to the edge of the Congo Craton. The seismic expression of the *Milelli et al*. [2012] model would be a vertical low velocity zone extending into the upper mantle, bounded by fast velocities associated with downwellings, which is consistent with shear wave velocity structure found by this study and by previous studies. Furthermore, the *Milelli et al*. [2012] instability model indicates that these features should extend into oceanic lithosphere, perpendicular to the continental margin, showing similar offshore structure to that observed onshore. Thus, the *Milelli et al*. [2012] model has the advantage of also providing an explanation for the offshore extension of the CVL, which was not imaged in this study due to the limitation of land instrumentation, regardless of the poorly defined spatial relationship between the western edge of the Congo Craton and the oceanic CVL.

6. Conclusions

Results from Rayleigh wave phase velocities and inversion for three-dimensional shear wave velocity structure give evidence for a vertical low velocity zone beneath the CVL that extends from the base of the crust to depths of at least 200 km, with the most pronounced low velocities found at depths shallower than 150 km. The model shows evidence that the lithospheric mantle has been highly eroded beneath the main branch of the CVL, and partially thinned beneath the northern branch, consistent with geochemical evidence for a sublithospheric source of CVL volcanics. Velocities are consistent along the line and do not show evidence for separate magma production centers at mantle depths along the CVL. A sharp vertical boundary separates these low velocities from fast velocities beneath the Congo Craton. Azimuthal anisotropy beneath the CVL is oriented roughly N-S, sub-perpendicular to the strike of the CVL, and indicating that mantle flow along the line is unlikely.

Based on these observations, we conclude that the most likely geodynamic origin for the CVL is one of two models. The first possible geodynamic mechanism is an edge-flow convection eddy driven by and parallel to the boundary between the thick lithosphere of the Congo Craton and thinner lithosphere to the north in the manner described by *King and Anderson* [1998]. The second potential mechanism is a lithospheric instability, driven by differential cooling of the thick continental lithosphere relative to the thinner oceanic lithosphere, and would be oriented perpendicular to the continental margin [*Milelli et al*., 2012].

Both the lithospheric instability model and the edge-flow convection model predict an upwelling in the upper mantle beneath the CVL and a downwelling beneath the edge of the Congo Craton, and both are consistent with our onshore seismic observations of a vertically oriented low velocity anomaly in the upper mantle beneath the CVL, separated by a vertical boundary from the fast velocities of the Congo Craton. However, because the edge-flow convection model predicts an upwelling parallel to the sharp change in lithospheric thickness at the edge of the Congo Craton, and because the spatial relationship between the

offshore CVL and the western edge of the craton is poorly defined, it is unclear whether an upwelling generated by this process alone could create both the onshore and offshore CVL. An upwelling generated by processes described by the lithospheric instability model, however, should be perpendicular to the continental margin both onshore and offshore, which is the case for the CVL and is not dependent on the location of the Congo Craton's western edge. Thus, an improved understanding of the offshore structure of the CVL and the position of the western edge of the Congo Craton may aid in distinguishing between these two candidate models for the formation of the CVL.

Acknowledgments
Funding for this study was provided by grants from the National Science Foundation EAR-0310094 and EAR-0310272. Data used in this study are archived at the IRIS Data Management Center under the network code XB and can be accessed through the IRIS website (http://www.iris.edu) without restrictions to researchers at IRIS member institutions. Maps were created using the Generic Mapping Tools package (http://gmt.soest.hawaii.edu/). We gratefully acknowledge the constructive comments of two anonymous reviewers.

References

Adams, A. N., and A. A. Nyblade (2011), Shear wave velocity structure of the southern African upper mantle with implications for the uplift of southern Africa, *Geophys. J. Int.*, *186*, 808–824, doi:10.1111/j.1365-246X.2011.05072.x.

Adams, A. N., A. A. Nyblade, and D. Weeraratne (2012), Upper mantle shear wave velocity structure beneath the East African plateau: Evidence for a deep, plateau wide low velocity anomaly, *Geophys. J. Int.*, *189*, 123–142, doi:10.1111/j.1365-246X.2012.05272.x.

Aka, F. T., K. Nagao, M. Kusakabe, and N. Nfomou (2009), Cosmogenic helium and neon in mantle xenoliths from the Cameroon Volcanic Line (West Africa): Preliminary observations, *J. Afr. Earth Sci.*, *55*, 175–184, doi:10.1016/j.jafrearsci.2009.04.002.

Aki, K., and P. Richards (2002), *Quantitative Seismology*, 2nd ed., pp. 403–406, Univ. Science Books, Sausalito, Calif.

Bassin, C., G. Laske, and G. Masters (2000), The current limits of resolution for surface wave tomography in North America, *Eos Trans. AGU*, *81*, F897.

Behn, M., C. Conrad, and P. Silver (2004), Detection of upper mantle flow associated with the African Superplume, *Earth Planet. Sci. Lett.*, *224*, 259–274.

Boukeke, D. (1994), Structures crustales d'Afrique Centrale déduites des anomalies gravimétriques et magnétiques: le domaine précambrien de la République Centrafricaine et du Sud Cameroun, PhD thesis, Univ. of Paries XI, Orsay.

Browne, J., and J. Fairhead (1983), Gravity study of the Central African Rift System: A model of continental disruption, 1, The Ngaoundere and Abu Gabra Rifts, *Tectonophysics*, *94*, 187–203.

Burke, K. (2001), Origin of the Cameroon Line of volcano-capped swells, *J. Geol.*, *109*(3), 349–362.

Burke, K., T. Dessauvagie, and A. Whiteman (1971), The opening of the Gulf of Guinea and the geological history of the Benue Trough and Niger delta, *Nat. Phys. Sci.*, *233*, 51–55.

Cornen, G., and R. C. Maury (1980), Petrology of the volcanic island of Annobón, Gulf of Guinea, *Mar. Geol.*, *36*(3–4), 253–267, doi:10.1016/0025-3227(80)90090-0.

Coulon, C., P. Vidal, C. Dupuy, P. Baudin, M. Popoff, H. Maluski, and D. Hermitte (1996), The Mesozoic to early Cenozoic magmatism of the Benue Trough (Nigeria); geochemical evidence for the involvement of the St Helena Plume, *J. Petrol.*, *37*(6), 1341–1358.

Daly, M. C., S. R. Lawrence, K. Diemu-Tshiband, and B. Matouana (1992), Tectonic evolution of the Cuvette Centrale, Zaire, *J. Geol. Soc. London*, *149*, 539–546.

De Plaen, R., I. Bastow, E. Chambers, D. Keir, R. Gallacher, and J. Keane (2014), The development of magmatism along the Cameroon Volcanic Line: Evidence from seismicity and seismic anisotropy, *J. Geophys. Res. Solid Earth*, *119*, 4233–4252, doi:10.1002/2013JB0105823.

Déruelle, B., C. Moreau, C. Nkoumbou, R. Kambou, J. Lissom, E. Njongfang, R. T. Ghogomu, and A. Nono (1991), The Cameroon Line, in *Magmatism in Extensional Structural Settings. The Phanerozoic African Plate*, edited by A. B. Kampunzu and R. T. Lubala, pp. 274–327, Springer, Berlin, Germany.

Déruelle, B., I. Ngounouno, and D. Demaiffe (2007), The 'Cameroon Hot Line' (CHL): A unique example of active alkaline intraplate structure in both oceanic and continental lithospheres, *C. R. Geosci.*, *339*, 589–600.

Dongmo, A., D. Nkouathio, A. Pouclet, J.-M. Bardintzeff, P. Wandji, A. Nono, and H. Guillou (2010), The discovery of late Quaternary basalt on Mount Bambouto: Implications for recent widespread volcanic activity in the southern Cameroon Line, *J.. Afr. Earth Sci.*, *57*, 96–108.

Dorbath, C., L. Dorbath, J. D. Fairhead, and G. W. Stuart (1986), A teleseismic delay time study across the Central African Shear Zone in the Adamawa region of Cameroon, West Africa, *Geophys. J. R. Astron. Soc.*, *86*(3), 751–766.

Druken, K., C. Kincaid, and R. Griffiths (2013), Directions of seismic anisotropy in laboratory models of mantle plumes, *Geophys. Res. Lett.*, *40*, 3544–3549, doi:10.1002/grl.50671.

Dunlop, H. M. (1983), Strontium isotope geochemistry and potassium-argon studies on volcanic rocks from the Cameroon Line, West Africa, PhD thesis, Univ. of Edinburgh, Edinburgh, U. K.

Dunlop, H. M., and J. G. Fitton (1979), K-Ar and Sr-isotopic study of the volcanic-rocks of the island of Prìncipe, West Africa—Evidence for mantle heterogeneity beneath the Gulf of Guinea, *Contrib. Mineral. Petrol.*, *71*(2), 125–131, doi:10.1007/BF00375428.

Ebinger, C., and N. Sleep (1998), Cenozoic magmatism throughout East Africa resulting from impact of a single plume, *Nature*, *295*, 788–791.

Elsheikh, A. A., S. S. Gao, and K. H. Liu (2014), Formation of the Cameroon Volcanic Line by lithospheric basal erosion: Insight from mantle seismic anisotropy, *J. Afr. Earth Sci.*, *100*, 96–108.

Fairhead, J. D., and C. S. Okereke (1987), A regional gravity study of the West African Rift System in Nigeria and Cameroon and its tectonic interpretation, *Tectonophysics*, *143*, 141–159.

Fairhead, J. D., and R. M. Binks (1991), Differential opening of the Central and South Atlantic Oceans and the opening of the West African rift system, *Tectonophysics*, *187*, 191–203.

Farnetani, C., and H. Samuel (2005), Beyond the thermal plume paradigm, *Geophys. Res. Lett.*, *32*, L07311, doi:10.1029/2005GL022360.

Fitton, J. G. (1980), The Benue Trough and Cameroon Line. A migrating rift system in West Africa, *Earth Planet. Sci. Lett.*, *51*, 132–138.

Fitton, J. G. (1987), The Cameroon Line, West Africa: A comparison between oceanic and continental alkaline volcanism, in *Alkaline Igneous Rocks*, *Geol. Soc. London Spec. Publ.*., vol. 30, edited by J. G. Fitton and B. G. J. Upton, pp. 273–291.

Fitton, J. G., and H. M. Dunlop (1985), The Cameroon Line, West Africa, and its bearing on the origin of oceanic and continental alkali basalt, *Earth Planet. Sci. Lett.*, *72*(123038), doi:10.1016/0012-821X(85)90114-1.

Forsyth, D., and A. Li (2005), Array analysis of two-dimensional variations in surface wave phase velocity and azimuthal anisotropy in the presence of multipathing interference, in *Seismic Earth: Array Analysis of Broadband Seismograms*, *Geophys. Monogr. Ser.*, vol. 157, edited by A. Levander and G. Nolet, pp. 81–97, Am. Geophys. Soc., Washington, D. C.

Friederich, W., and E. Wielandt (1995), Interpretation of seismic surface waves in regional networks: Joint estimation of wavefield geometry and local phase velocity: Method and tests, *Geophys. J. Int.*, *120*, 731–744.

Gallacher, R. J., and I. D. Bastow (2012), The development of magmatism along the Cameroon Volcanic Line: Evidence from teleseismic receiver functions, *Tectonics*, *31*, TC3018, doi:10.1029/2011TC003028.
Grant, N. K., D. C. Rex, and S. J. Freeth (1972), Potassium-argon ages and strontium isotope ration measurements from volcanic rocks in northeastern Nigeria, *Contrib. Mineral. Petrol.*, *35*(4), 277–292, doi:10.1007/BF00371310.
Grunau, H., P. Lehner, M. Cleintuar, P. Allenbach, and G. Bakker (1975), New radiometric ages and seismic data from Fuerteventura (Canary Islands), Maio (Cape Verde Islands), and São Tomé (Gulf of Guinea), in *Progress in Geodynamics: Proceedings of the National Symposium on Geodynamics Held in Amsterdam, April 3–4, 1975*, edited by G. J. Borradaile et al., pp. 90–118, North-Holland Co., New York.
Harmon, N., D. Forsyth, D. Weeraratne, Y. Yang, and S. Webb (2011), Mantle heterogeneity and off axis volcanism on young Pacific lithosphere, *Earth Planet. Sci. Lett.*, *311*, 306–315.
Hedberg, J. (1969), A geological analysis of the Cameroon trend, PhD thesis, Princeton Univ., Princeton, New Jersey.
Heeszel, D. S., D. A. Wiens, A. A. Nyblade, S. E. Hansen, M. Kanao, M. An, and Y. Zhao (2013), Rayleigh wave constraints on the structure and tectonic history of the Gamburtsev Subglacial Mountains, East Antarctica, *J. Geophys. Res. Solid Earth*, *118*, 2138–2153, doi:10.1002/jgrb.50171.
Herrmann, R. B., and C. J. Ammon (2002), *Computer Programs in Seismology: Surface Waves, Receiver Functions and Crustal Structure*, p. 110, St. Louis Univ, St. Louis, Mo.
Julia, J., C. Ammon, R. Herrmann, and A. Correig (2000), Joint inversion of receiver function and surface wave dispersion observations, *Geophys. J. Int.*, *143*, 99–112.
Kamgang, P., E. Njonfang, A. Nono, D. Gountie, and F. Tchoua (2010), Petrogenesis of a silicic magma system: Geochemical evidence from Bamenda Mountains, NW Cameroon, Cameroon Volcanic Line, *J. Afr. Earth. Sci.*, *58*, 285–304.
Kennett, B., and E. Engdahl (1991), Traveltimes for global earthquake location and phase identification, *Geophys. J. Int.*, *105*, 429–465.
Kennett, B., E. Engdahl, and R. Bulard (1995), Constraints on seismic velocities in the Earth from travel times, *Geophys. J. Int.*, *122*, 108–124, doi:10.1111/j.1365-246X.1995.tb03540.x.
King, S., and J. Ritsema (2000), African hot spot volcanism: Small-scale convection in the upper mantle beneath cratons, *Science*, *290*, 1137–1140.
King, S. D., and D. L. Anderson (1995), An alternative mechanism of flood basalt formation, *Earth Planet. Sci. Lett.*, *136*, 269–279.
King, S. D., and D. L. Anderson (1998), Edge-driven convection, *Earth Planet. Sci. Lett.*, *160*, 289–296.
Koch, F. W., D. A. Wiens, A. A. Nyblade, P. J. Shore, R. Tibi, B. Ateba, C. T. Tabod, and J. M. Nnange (2012), Upper-mantle anisotropy beneath the Cameroon Volcanic Line and Congo Craton from shear wave splitting measurements, *Geophys. J. Int.*, *190*, 75–86, doi:10.1111/j.1365-246X.2012.05497.x.
Lee, D.-C., A. N. Halliday, J. G. Fitton, and G. Poli (1994), Isotopic variations with distance and time in the volcanic islands of the Cameroon line: Evidence for a mantle plume origin, *Earth Planet. Sci. Lett.*, *123*, 119–138.
Maluski, H., C. Coulon, M. Popoff, and P. Baudin (1995), 40Ar/39Ar chronology, petrology and geodynamic setting of Mesozoic to early Cenozoic magmatism from the Benue Trough, Nigeria, *J. Geol. Soc. London*, *152*, 311–326.
Marzoli, A., P. Renne, E. Piccirillo, C. Francesca, G. Bellieni, A. Melfi, J. Nyobe, and J. N'ni (1999), Silicic magmas from the continental Cameroon Volcanic Line (Oku, Bambouto and Ngaoundere): 40Ar-39Ar dates, petrology, Sr-Nd-O isotopes and their petrogenetic significance, *Contrib. Mineral. Petrol.*, *135*, 133–150.
Marzoli, A., E. Piccirillo, P. Renne, G. Bellieni, M. Iacumin, J. Nyobe, and A. Tongwa (2000), The Camberoon Volcanic Line revisited: Petrogenesis of continental basaltic magmas from lithospheric and asthenospheric mantle sources, *J. Petrol.*, *41*, 87–109.
Meyers, J. B., and B. R. Rosendahl (1991), Seismic reflection character of the Cameroon volcanic line: Evidence for uplifted oceanic crust, *Geology*, *19*, 1072–1076.
Meyers, J. B., B. R. Rosendahl, C. G. A. Harrison, and Z.-D. Ding (1998), Deep-imaging seismic and gravity results from the offshore Cameroon Volcanic Line, and speculation of African hotlines, *Tectonophysics*, *284*, 31–63.
Milelli, L., L. Fourel, and C. Jaupart (2012), A lithospheric instability origin for the Cameroon Volcanic Line, *Earth Planet. Sci. Lett.*, *335-336*, 80–87, doi:10.1016/j.epsl.2012.04.028.
Montelli, R., G. Nolet, F. Dahlen, G. Masters, E. Engdahl, and S. Hung (2004), Finite-frequency tomography reveals a variety of plumes in the mantle, *Science*, *303*, 338–343, doi:10.1126/science.1092485.
Morgan, W. J. (1983), Hotspot tracks and the early rifting of the Atlantic, *Tectonophysics*, *94*, 123–139.
Ngako, V., E. Njonfang, F. Aka, P. Affaton, and J. Nnange (2006), The North-South Paleozoic to Quaternary trend of alkaline magmatism from Niger-Nigeria to Cameroon: Complex interaction between hotspots and Precambrian faults, *J. Afr. Earth. Sci.*, *45*, 241–256.
Ngounouno, I., B. Déruelle, D. Demaiffe, and R. Montigny (1997), New data on the Cenozoic volcanism of the Garoua valley (Upper Benue trough, northern Cameroon), *C. R. Acad. Sci., Ser. II*, *325*(2), 87–94.
Ngounouno, I., B. Déruelle, D. Demaiffe, and R. Montigny (2001), Petrology of the alkaline undersaturated complex of Kokoumi (Cameroon), *Bull. Soc. Geol. France.*, *172*(6), 675–686, doi:10.2113/172.6.675.
Ngounouno, I., B. Déruelle, D. Demaiffe, and R. Montigny (2003), The monchiquites from Tchircotche, Upper Benue valley (northern Cameroon), *C. R. Geosci.*, *335*(3), 289-296, doi: 10.1016/S1631-0713(03)00047-6
Ngounouno, I., B. Déruelle, R. Montigny, and D. Demaiffe (2005), Petrology and geochemistry of monchiquites from Tchircotche (Garoua rift, north Cameroon, Central Africa), *Mineral. Petrol.*, *83*(3–4), 167–190, doi:10.1007/s00710-004-0068-y.
Ngounouno, I., B. Déruelle, R. Montigny, and D. Demaiffe (2006), The camptonites from Mount Cameroon, Cameroon, Africa, *C. R. Geosci.*, *338*(8), 537–544, doi:10.1016/j.crte.2006.03.015.
Njilah, I., H. Ajonina, D. Kamgang, and M. Tchindjang (2004), K-Ar ages, mineralogy, major and trace element geochemistry of the Tertiary-Quaternary lavas from the Ndu Volcanic Ridge N.W. Cameroon, *Afr. J. Sci. Technol.*, *5*(1), 47–56.
Njome, M. S., and M. J. de Wit (2014), The Cameroon Line: Analysis of an intraplate magmatic province transecting both oceanic and continental lithospheres: Constraints, controversies and models, *Earth Sci. Rev.*, *139*, 168–194.
O'Donnell, J.-P., A. Adams, A. Nyblade, G. Mulibo, and F. Tugume (2013), The uppermost mantle shear wave velocity structure of eastern Africa from Rayleigh wave tomography: Constraints on rift evolution, *Geophys. J. Int.*, doi:10.1093/gji/ggt135.
Plomerová, J., V. Babuska, C. Dorbath, L. Dorbath, and R. J. Lillie (1993), Deep lithospheric structure across the Central African Shear Zone in Cameroon, *Geophys. J. Int.*, *115*, 381–390.
Poudjom Djomani, Y. H., J. M. Nnange, M. Diament, C. J. Ebinger, and J. D. Fairhead (1995), Effective elastic thickness variations in west-central Africa inferred from gravity data, *J. Geophys. Res.*, *100*(B11), 22,047–22,070, doi:10.1029/95JB01149.
Poudjom Djomani, Y. H., M. Diament, and M. Wilson (1997), Lithospheric structure across the Adamawa plateau (Cameroon) from gravity studies, *Tectonophysics*, *273*, 317–327.
Press, W., S. Teukolsky, W. Vetterling, and B. Flannery (1992), *Numerical Recipes in FORTRAN: The Art of Scientific Computing*, 2nd ed., Cambridge Univ. Press, Cambridge, U. K.

Princivalle, F., G. Salviulo, A. Marzoli, and E. Piccirillo (2000), Clinopyroxene of spinel-peridotite mantle xenoliths from Lake Nji (Cameroon Volcanic Line, W Africa): Crystal chemistry and petrological implications, *Contrib. Mineral. Petrol.*, *139*, 503–508.

Reusch, A. M., A. A. Nyblade, D. A. Wiens, P. J. Shore, B. Ateba, C. T. Tabod, and J. M. Nnange (2010), Upper mantle structure beneath Cameroon from body wave tomography and the origin of the Cameroon Volcanic Line, *Geochem. Geophys. Geosyst.*, *11*, Q10W07, doi:10.1029/2010GC003200.

Reusch, A., A. Nyblade, R. Tibi, D. Wiens, P. Shore, A. Bekoa, C. Tabod, and J. Ngange (2011), Mantle transition zone thickness beneath Cameroon: Evidence for an upper mantle origin for the Cameroon Volcanic Line, *Geophys. J. Int.*, *187*, 1146–1150, doi:10.1111/j.1365-246X.2011.05239.x.

Ritsema, J., and H. J. van Heijst (2000), New seismic model of the upper mantle beneath Africa, *Geology*, *28*, 63–66.

Saito, M. (1981), DISPER80: A subroutine package for the calculation of seismic normal-mode solutions, in *Seismological Algorithms: Computational Methods and Computer Programs*, edited by D. J. Doornbos, Acad. Press Limited, New York.

Shapiro, N., and M. Ritzwoller (2002), Monte-Carlo inversion for a global shear-velocity model of the crust and upper mantle, *Geophys. J. Int.*, *151*, 88–105, doi:10.1046/j.1365-246X.2002.01742.x.

Stuart, G. W., J. D. Fairhead, L. Dorbath, and C. Dorbath (1985), A seismic refraction study of the crustal structure associated with the Adamawa Plateau and Garoua Rift, Cameroon, West Africa, *Geophys. J. R. Astron. Soc.*, *81*, 1–12.

Tarantola, A., and B. Valette (1982), Generalized non-linear problems solved using the least-squares criterion, *Rev. Geophys. Space Phys.*, *20*, 219–223.

Tibi, R., A. M. Larson, A. A. Nyblade, P. J. Shore, D. A. Wiens, J. M. Nnange, C. Tabod, and A. Bekoa (2005), A broadband seismological investigation of the Cameroon Volcanic Line, *Eos Trans. AGU*, *86*(52), Fall Meet. Suppl., Abstract S11B-0170.

Tokam, A.-P. K., C. T. Tabod, A. A. Nyblade, J. Julià, D. A. Wiens, and M. E. Pasyanos (2010), Structure of the crust beneath Cameroon, West Africa, from the joint inversion of Rayleigh wave group velocities and receiver functions, *Geophys. J. Int.*, *183*, 1061–1076, doi:10.1111/j.1365-246X.2010.04776.x.

Van Houten, F. B. (1983), Sirte Basin, north-central Libya: Cretaceous rifting above a fixed mantle hotspot?, *Geology*, *11*, 115–118.

Vicat, J., J. Leger, E. Nsifa, P. Piguet, J. Nzenti, R. Tchameni, and A. Pouclet (1996), Distinction within the Congo craton in South-West Cameroon of two doleritic episodes initiating the Eburnean (Paleoproterozoic) and Pan-African (Neoproterozoic) orogenic cycles, *C.R. Acad. Sci., Ser. IIa: Sci. Terre Planets*, *323*, 575–582.

Weeraratne, D., D. Forsyth, K. Fischer, and A. Nyblade (2003), Evidence for an upper mantle plume beneath the Tanzanian craton from Rayleigh wave tomography, *J. Geophys. Res.*, *108*(B9), 2427, doi:10.1029/2002JB002273.

Yang, Y., and D. Forsyth (2006), Regional tomographic inversion of the amplitude and phase of Rayleigh waves with 2-D sensitivity kernels, *Geophys. J. Int.*, *166*, 1148–1160.

Zhou, Y., F. Dahlen, and G. Nolet (2004), Three dimensional sensitivity kernels for surface wave observables, *Geophys. J. Int.*, *158*, 142–168.